# Chain collapse and interfacial slip of polystyrene films in good/non-solvent vapor mixtures

| | |
|---|---|
| Journal: | *Macromolecules* |
| Manuscript ID | ma-2015-02253t.R1 |
| Manuscript Type: | Article |
| Date Submitted by the Author: | n/a |
| Complete List of Authors: | Al-Khayat, Omar; University of Sydney, School of Chemistry<br>Geraghty, Kieran; University of Sydney, School of Chemistry<br>Shou, Keyun; University of Sydney, School of Chemistry<br>Nelson, Andrew; ANSTO, Bragg Institute<br>Neto, Chiara; University of Sydney, School of Chemistry |
| | |

# For Table of Contents Only

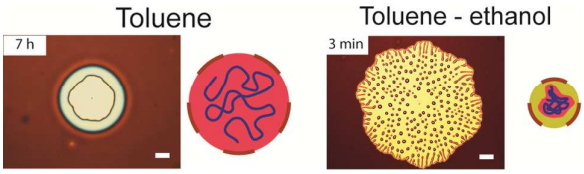

# Chain collapse and interfacial slip of polystyrene films in good/non-solvent vapor mixtures

*Omar Al-Khayat,[1] Kieran Geraghty,[1] Keyun Shou,[1] Andrew Nelson,[2] Chiara Neto[1,]**

[1]School of Chemistry, The University of Sydney, NSW 2006 Australia

[2] Bragg Institute, Australian Nuclear Science and Technology Organisation, Locked Bag 2001, Kirrawee DC, NSW 2232, Australia,

* Corresponding author: chiara.neto@sydney.edu.au

## Abstract

We investigated the dynamics and morphology of dewetting of metastable polystyrene films (thickness 75 - 500 nm) cast on silicon substrates, upon exposure to vapors of a mixture of toluene, a good solvent, and ethanol, a non-solvent. Adding more than 2% weight ethanol to the saturated toluene environment resulted in a dramatic increase in dewetting rate, an increase in the contact angle of polymer droplets and hole rims on the substrate, and to extensive fingering leading to droplet shedding. Films pre-annealed close to $T_g$ before exposure to the solvent vapors showed markedly slower dewetting. We conclude that, in the presence of a good/non-solvent mixture, the polymer chains transition to a globule conformation, which leads to larger interfacial slip, lower viscosity, and significant elastic stress. The slip length derived in the presence of ethanol vapor is close to the values obtained for polystyrene on hydrophobised silicon. As the dewetting process is so significantly boosted by exposure to mixed toluene/ethanol vapors, polystyrene films as thick as 520 nm could be dewetted.

## Introduction

The dewetting of thin polymer films from a solid substrate has been studied extensively over the past three decades,[1-7] and has interesting applications in surface

patterning.[8, 9] Our group has demonstrated applications of polymer dewetted patterns in protein and cell patterning[10-12] and in atmospheric water capture.[13]

In most unstable and metastable polymer liquid films (thickness < 100 nm) dewetting occurs by nucleation of holes at random locations, whereby the substrate is exposed and the polymer removed accumulates in a rim around each hole.[14] With time the holes grow in diameter, the rims of neighboring holes coalesce into liquid cylinders, and finally into isolated droplets of the polymer on the substrate. Dewetted holes have often circular shape and regular rims, but, in cases where interfacial slip is strong, undulations of the rim shape lead to fingering and droplet shedding.[7, 15-21] One of the main causes of dewetting is the unfavorable interfacial interactions of the liquid film at the solid surface. For example, one proposed form of the interfacial potential $\Phi(h)$, Equation 1, includes the effects of short-range forces (first term) and long-range van der Waals forces (two following terms) for polystyrene films of thickness $h$ on top of silicon substrates coated with silicon oxide of thickness $d$, with Hamaker constants $A_{Si}$ (negative) and $A_{SiO}$ (positive).[14] In the case of a thick oxide layer (thickness $d$ of 200 nm), this expression correctly predicts a van der Waals attraction which promotes film dewetting.

$$\varphi(h) = \frac{c}{h^8} - \frac{A_{SiO}}{12\pi h^2} + \frac{A_{SiO} - A_{Si}}{12\pi(h+d)^2} \quad (1)$$

When polar interactions are important, i.e. when either the film or the fluid environment in which it is immersed are polar, polar attractions also contribute to increasing the driving force for film dewetting.[22, 23] The polar contribution often takes the form $S_p \, exp\left(-\frac{h}{l}\right)$, where $S_p$ is the polar component of spreading coefficient, and $l$ is a correlation length.

In the past 10 years there has been increased understanding of another important driving force for dewetting, the chain equilibration process in thin films.[24-31] Spin-coating induces strongly out-of-equilibrium conformations of the chains and low entanglement density due to the fast evaporation of the solvent. This leads to residual elastic stresses that relax upon annealing, and drastically affect dewetting rate,[27-29] entanglement density and viscosity,[32] and thermal expansion.[25, 33-35] Although annealing of polymer films by exposure to solvent vapors of different quality has been explored before,[33-40] there has not been a systematic study of how

solvent quality affects dewetting, and in particular the elastic forces within the polymer film.

Here we have observed the effect of gradually changing the quality of the solvent used for annealing polystyrene (PS) films of thickness 75 - 500 nm on top of silicon wafers with a native (1.8 nm thick) oxide layer, a system that thermally does not dewet, as the van der Waals driving force in Eq. (1) is weak in this system. The films dewetted very slowly in a good solvent (toluene) vapor, where the PS chains assume a loose, open coil conformation.[41, 42] However, the PS films dewetted readily in a mixture of the vapor of a good solvent (toluene) and a non-solvent (ethanol), and the results highlight the role of elastic recoiling forces. In pure ethanol the PS chains are completely insoluble and hardly even swell, assuming a compact globule conformation through volume interactions,[43] but in mixtures of toluene and ethanol the chain behavior is more complicated and somewhat paradoxical.[44, 45] The preferential adsorption of the toluene in the vapor mixture leads to a strong collapse of the chains, so that, compared to the pure good solvent case, an overall shrinking of the polymer chains is observed. Although this behavior has been predicted by Monte-Carlo calculations in pioneering work by Magda et al.,[45] and observed in scattering experiments in dilute regimes,[42, 43, 46] or on brushes,[47] this is the first demonstration of how thoroughly the addition of the non-solvent affects dewetting morphology, dewetting rate, and dewetting mechanism.

# Experimental

Polystyrene films of thickness 75 – 100 nm (PS96k, $M_w$ = 96 kg/mol, $M_w/M_n$ = 1.01, Polymer Standards Service) were spin-coated (20 - 30 mg/mL in toluene, Laurell Technologies) on prime grade silicon wafers coated with a native oxide layer (1.8 ± 0.2 nm thick, MMRC Pty. Ltd., Australia). To induce dewetting, the PS films were placed in a saturated vapor environment of mixtures of toluene and ethanol, varying the weight ratio of the solvents in the liquid phase, in a custom-designed Teflon cell (Figure 1), which allows for *in situ* observation of dewetting by optical microscopy (Nikon Eclipse LV150). Thicker films (thickness 100 - 500 nm) were prepared by dip coating (KSV, NIMA) the wafers in a PS192k solution ($M_w$ = 192 kg/mol, Sigma Aldrich, 26 – 61 mg/mL in toluene, lowered at 100 mm/min).

Prior to film preparation, the silicon wafers were thoroughly cleaned by sonication in ethanol and acetone, blow dried in pure nitrogen, then exposed to a $CO_2$ snow jet gun to remove particulate contaminants (Applied Surface Technologies, NJ, USA), and air plasma for 1 min (Harrick Plasma, Itacha NY, model PDC-002).

Spectroscopic ellipsometry (J.A. Woollam Co. Inc., M2000V) and x-ray reflectometry (Panalytical X'Pert Pro, operating at 8.048 keV) were used to establish film thickness, with measurements over three points on each sample. Atomic force microscopy (AFM, Bruker, Multimode 8) was used to characterize hole morphology and to measure the contact angle of the isolated PS droplets on the substrate at the end of dewetting. The quality of the solvents for PS was estimated using Hansen Solubility Parameters (Table S1, Supporting Information).

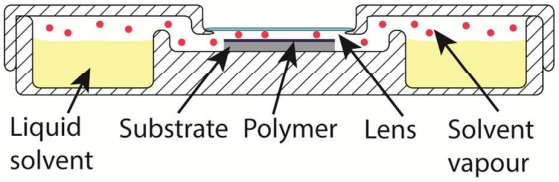


Figure 1: Schematic diagram of the Teflon cell used to observe *in situ* the dewetting of polystyrene films by solvent vapors. The Teflon cell has a port open to the atmosphere to allow solvent injection and pressure equilibration. A microscope cover lens is situated above the sample for observation using optical microscopy.

## Results

The Hansen solubility parameters[48] for the solvent/PS used in this study are listed in Table S1 in Supporting Information, SI. Table S1 indicates that toluene is a good solvent for polystyrene, whereas ethanol is a non-solvent. Toluene and ethanol are entirely miscible and were mixed in the liquid phase inside the custom-designed Teflon chamber depicted in Figure 1 in different weight proportions (99:1, 95:5, 90:10, 85:15, 60:40, and 40:60 wt. toluene/ethanol). The mole fraction of each component in the vapor phase is known,[49] and shown in Table S2 in SI. However, for clarity, from now on we will refer directly to the weight composition of the liquid mixture.

As shown in Figure S1 in SI, thermal annealing of the prepared PS96k films at 180 °C (above the $T_g$ = 100 °C for bulk PS)[50] for long periods of time (> 65 h) increased the surface roughness, but did not initiate film dewetting from the substrate, due to the small van der Waals driving force.[14]

Upon exposure to the solvent vapor environment, the PS96k films immediately changed color due to swelling. X-ray reflectometry data, Figure 2, showed that a 78 ± 0.5 nm PS96k film swelled to 109 nm in the saturated toluene vapor (a thickness increase of 31 nm, 40% of the initial thickness). Using the empirical rule that 1% of toluene lowers the $T_g$ by 5 °C,[51] the increase in chain mobility was dramatic, leading to a $T_g$ below room temperature. In contrast, upon exposure to vapors of a 30:70 (w/w) toluene/ethanol mixture, the swelling of the PS film was only 20 nm, 65% of the value obtained in pure toluene. The swelling of the same film in pure ethanol vapor was just 3 nm. This information will be used later to explain the observed dewetting behavior.

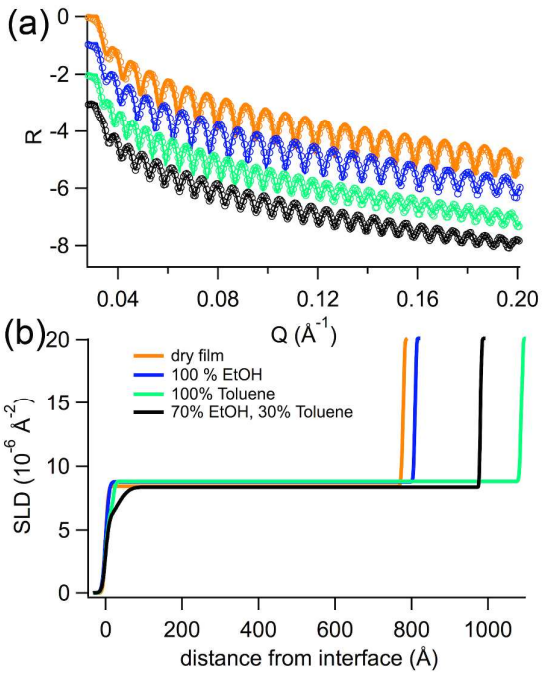


Figure 2 (a) X-ray reflectivity profiles from solvent swollen PS96k films. Experimental data (empty circles) and fits (lines) are shown. From top to bottom the lines correspond to: as prepared (dry) PS film (orange), film annealed on 100% ethanol (blue), film annealed in 100% toluene (green), and annealed in 70:30 toluene/ethanol (black). (b) Corresponding scattering length density (SLD) profiles.

***Overview on the effect of annealing in good/non-solvent vapor mixture***

Annealing the PS96k films in pure toluene resulted in a very slow dewetting process, as expected due to the small van der Waals driving force[14] (Figures 3a-d): few holes nucleated and grew slowly, reaching the size of 100 μm after two hours of toluene vapor annealing. Complete dewetting into isolated droplets occurred only after 3 days

of annealing. The nucleated holes had irregular shape, and jagged hole rims, that led to irregular, wide fingers, which did not develop into droplets. In comparison, thermal dewetting of the same PS films on an underlying P4VP film led to regular, circular holes (data now shown).

The addition of the saturated vapors of ethanol to the annealing environment resulted in much faster dewetting of the PS96k films. In 85:15 toluene/ethanol mixture, the PS96k film dewetted completely within 10 minutes (Figures 3(e-h)). Upon addition of more than 1% (w/w) ethanol, the hole rims became unstable in all cases, leading to numerous and regular fingers, which pinched off and shed numerous droplets inside the growing hole (Figure 3). In contrast, in the case of pure toluene annealing, isolated polymer droplets were only formed upon coalescence of adjacent holes, and the droplets were found not inside the holes, but on lines of coalescence of neighboring holes.

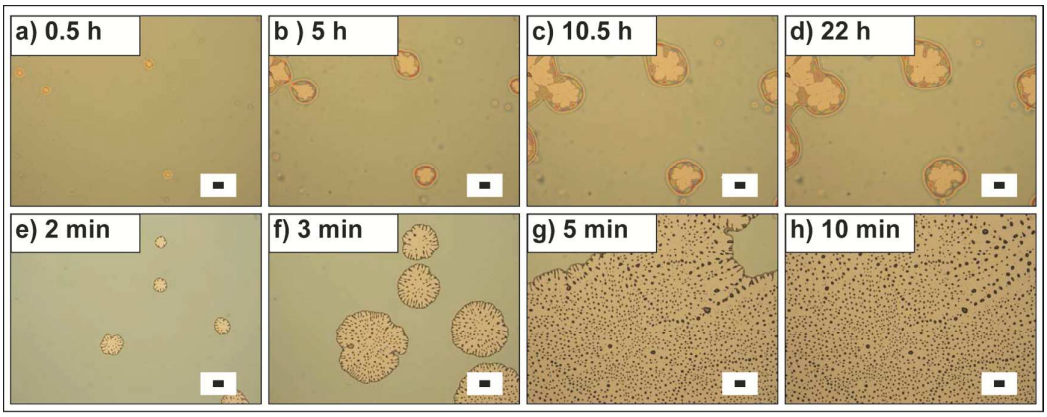


Figure 3: Representative optical micrographs of *in situ* annealing of PS 96k thin films (75 ± 0.8 nm), at room temperature (23 ± 1 °C), (a-d) dewetting in the saturated vapor of toluene; and (e-h) in a mixture of 85:15 (w/w) toluene and ethanol vapor. Time stamps indicate time since start of vapor annealing. Scale bars = 100 µm.

### *Rim morphology*

The morphology of rims around dewetted holes was strikingly dependent on annealing solvent, as shown in Figure 4, which compares two hole rims of similar width ≈ 40 µm, formed in pure toluene (part a) and in 80:20 (w/w) toluene/ethanol mixture (b). The rim obtained in pure toluene was low and wide, with low contact angle of 2° - 4° on top of the silicon wafer (Figure 4c; also discussed later in Table 1); the hole at this stage was still round and regular in shape, with minimal fingering, and

the rim width $w$ increased slowly (Figure S2), and linearly with increasing hole radius, $w \propto 0.33\ r$ (Figure 4d, blue diamonds).

Upon the addition of 5% wt. (or greater) ethanol, the rim grew much faster (Figure S2), reaching a much higher aspect ratio (six times greater height for a rim of similar width, approximately 1200 nm versus 200 nm in pure toluene, Figures 4b and c) and higher contact angle (9° - 14°). From a width of less than 8 μm the rim developed periodic undulations along the circumference, with some portions becoming thicker and elongated (cross section *i*, Figure 4c), and some portions becoming thinner and narrower (cross section *ii*, Figure 4c). The thick elongated portions formed fingers, which repeatedly formed a neck and broke up into droplets. The average rim width (averaged over the whole circumference) followed a linear growth with hole radius, $w \propto 0.04\ r$ (Figure 4d, green triangles). The labels **I**, **II**, and **III** on the data for the 95:5 and 99:1 wt. mixtures correspond to the optical micrographs in Figure 6c, which identify the first captured dewetted hole (**I**), the stage when the rim is well established (**II**), and the stage when undulations (for the 99:1 case) or fingering (for the 95:5 case) were well established (**III**).

The observation of large undulations of the rim width are indicative of a dewetting mechanism dominated by interfacial slip of the melt at the solid substrate.[19] Upon addition of ethanol in the annealing atmosphere, ethanol molecules likely adsorbed to the silicon oxide substrate, increasing the interfacial slip of the PS on top of the ethanol layer. This effect was clear at 5% wt ethanol, but already observable at a reduced level at 1% wt. ethanol: the undulations in the rim width became more frequent than those observed in pure toluene (see micrographs in Figure 6c). For both 90:10 and 60:40 wt. toluene/ethanol proportions, the rim width was similar and reached an averaged constant value at early stages. Figure S2 shows the same rim width data as in Figure 4 plotted against time, and highlights how much faster the maturation of the rim became in the presence of ethanol.

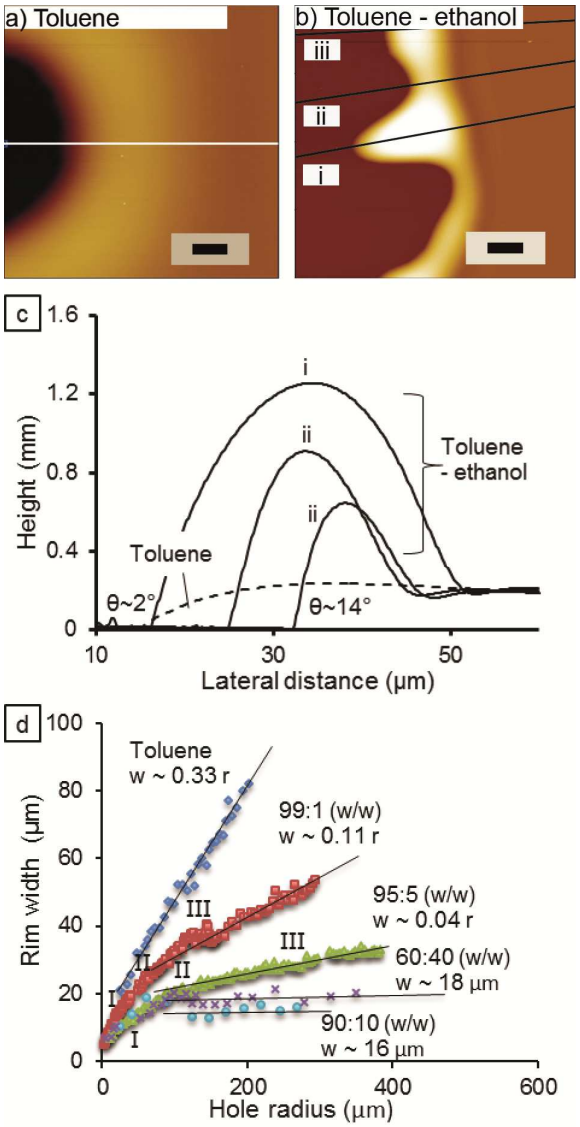


Figure 4: AFM micrographs of the rim surrounding a hole in PS96k films (154.8 ± 0.7 nm thick) annealed in saturated (a) toluene vapor, height scale 400 nm; (b) 80:20 (w/w) toluene/ethanol mixture, height scale 1400 nm, scale bars 20 μm. (c) AFM cross-sections of hole rims, showing the receding contact angle (error ± 2°) of the rims on the substrate (dashed line for toluene, solid line for toluene/ethanol); sections *i* – *iii* were taken along the lines indicated in part (b). (d) Hole rim width versus hole radius for PS96k films (75 ± 0.8 nm) annealed in saturated toluene (blue diamonds), 99:1 (red squares), 95:5 (green triangles), 90:10 (blue circles) and 60:40 (purple crosses) (w/w) toluene/ethanol mixtures. Roman numerals refer to the micrograph sequences for 99:1 and 95:5 in Figure 6c. The standard deviation in the data points is smaller than the size of the symbols.

### *Droplet morphology*

The PS droplets found on the silicon substrate at the end of dewetting in pure toluene vapors were irregular in shape, appearing pinned to the substrate (Figure 5a), while they were nicely round and regular upon addition of 15 % wt. ethanol (Figure 5b).

The contact angle, distribution density and diameter of the PS droplets measured from optical micrographs are shown in Table 1. The PS droplets produced from rim instabilities with 15% wt. ethanol vapor present were much smaller than those in pure toluene (average 13 μm compared with 21 μm), and more numerous (746 $mm^{-2}$ compared with 50 $mm^{-2}$). The contact angle of PS droplets on the silicon substrate was higher (25° ± 2°) when the films were annealed in the presence of 15% wt. ethanol, compared to the pure toluene vapors (4° ± 2°, Figure 5c, and Table 1). Adding 15% ethanol into the annealing vapor decreased the spreading parameter of PS on the substrate by one order of magnitude compared to annealing thermally and in pure toluene (Table 1). This effect can be explained with the polar interactions between ethanol and silicon oxide, which reduced the spreading of PS, and increased its dewetting rate.

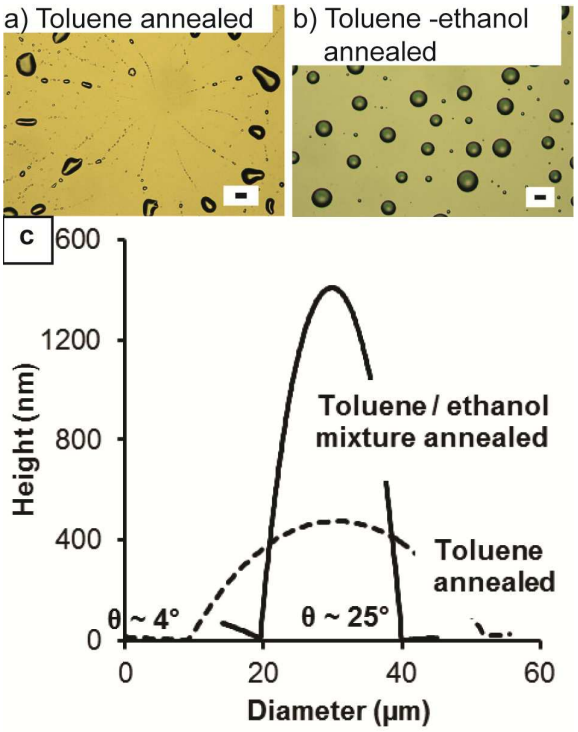


Figure 5: Optical micrographs of isolated PS96k droplets after completely dewetting 97 ± 1 nm thin polystyrene films at room temperature (23 ± 1 °C) in (a) saturated toluene vapors. Scale bar = 100 μm; (b) 85: 15 (w/w) toluene/ethanol mixture. Scale bar = 20 μm. (c) *Ex situ* AFM cross sections of PS96k droplets dewetted under toluene annealing (broken line), and 85:15 (w/w) toluene/ethanol mixture annealing (solid line), with indicated contact angle.

Table 1: Contact angle, diameter, deviation from the mean diameter, and distribution density of the isolated PS96k droplets after annealing a 97 nm thick films in solvent vapors. The spreading parameter is calculated from $S = \gamma_{PS} \cos(\theta - 1)$, where $\gamma$ is the surface tension of PS (41 mN/m at 20 ˚C)[52] and $\theta$ is the contact angle of PS droplets on silicon oxide/ silicon substrates.

| Annealing procedure | Contact angle (°) | Droplet diameter (μm) | Deviation from mean diameter (μm) | Droplet density ($mm^{-2}$) | Spreading parameter (mN/m) |
|---|---|---|---|---|---|
| Thermal above $T_g$ | 7.5 ± 5 [a] | - | - | - | -0.35 |
| Toluene vapor | 4 ± 1 | 21 ± 2 | 25 | 50 | -0.10 |
| 85:15 (w/w) toluene/ethanol vapors | 25 ± 2 | 13 ± 1 | 3 | 746 | -3.8 |

[a] Literature value obtained by dewetting thermally a PS film on a 200 nm thick silicon oxide layer on silicon.[53]

### *Dewetting rate*

It is obvious from Figure 6 that film dewetting became much faster upon addition of ethanol vapor to toluene vapor. The dewetting rate reached a maximum at 15% wt. ethanol, and decreased again at values higher than 15% wt., until no dewetting was observed in pure ethanol vapor (inset of Figure 6a).[54]

Figures 6a and 6b illustrate the growth of the diameter of the dewetted holes, *D,* versus time, *t*, and the dewetting velocity versus hole radius, respectively, until hole coalescence or until the holes grew outside the frame. In all annealing conditions, in the early stage $D \propto t^{2/3 \pm 0.1}$, characteristic of a regime where interfacial slip of the polymer at the solid surface is the dominating mechanism.[16, 55] In a later stage, $D \propto t^{1 \pm 0.1}$, characteristic of a regime where dissipation takes place mainly by viscous flow within the rim. The transition between these two regimes is clearly visible in Figure 6a for the pure toluene case (blue diamonds with dashed line and solid line fit) and the 99:1 toluene/ethanol case (red squares with line), while it cannot be appreciated for the 95:5 and 40:60 case, as it occurs at shorter times and smaller hole radius. This transition between slip and viscous dissipation is well known for polymer thin films dewetting.[16, 17, 55] It is expected that in the case of interfacial slip the frictional forces are proportional to the size of the moving rim, so that when a critical rim size is reached, interfacial slip becomes a minor contributor to dewetting, and the dewetting rate becomes dominated by the viscous dissipation within the rim.[17] From the

characteristic time of this transition, an estimate of the slip length and reptation times can be derived, as shown in the Discussion Section below (Table 2).

The change in rim width over time (Figure 4d) can be matched up with the change in dewetting velocity (Figure 6b), and the appearance of rim undulations (Figure 6c). For the 99:1 wt. toluene/ethanol case, the dewetting rate decreased steadily in the initial stages (stages **I** - **II**), while the rim width was still growing, and undulations in the transverse direction were starting to grow (Figure 6c). Once the rim width growth slowed down and the undulations in rim width reached a steady state (stage **III**), the dewetting rate also reached a constant value ($v \approx 0.02$ μm/s at a hole radius of 160 μm, stage **III**), corresponding to the transition from a slip regime to dynamics dominated by viscous dissipation.[16]

In the 95:5 wt. toluene/ethanol case, the dewetting velocity initially grew with time while the hole was opening up (up to stage **I**) and fingering was developing (stages **II**), and then reached an average constant value in correspondence to the stage where fingering and droplet shedding also reached an established steady state (stage **III**).[56] This correspondence between rim width growth and dewetting rate is also clearly illustrated in Figures S4 – S6.

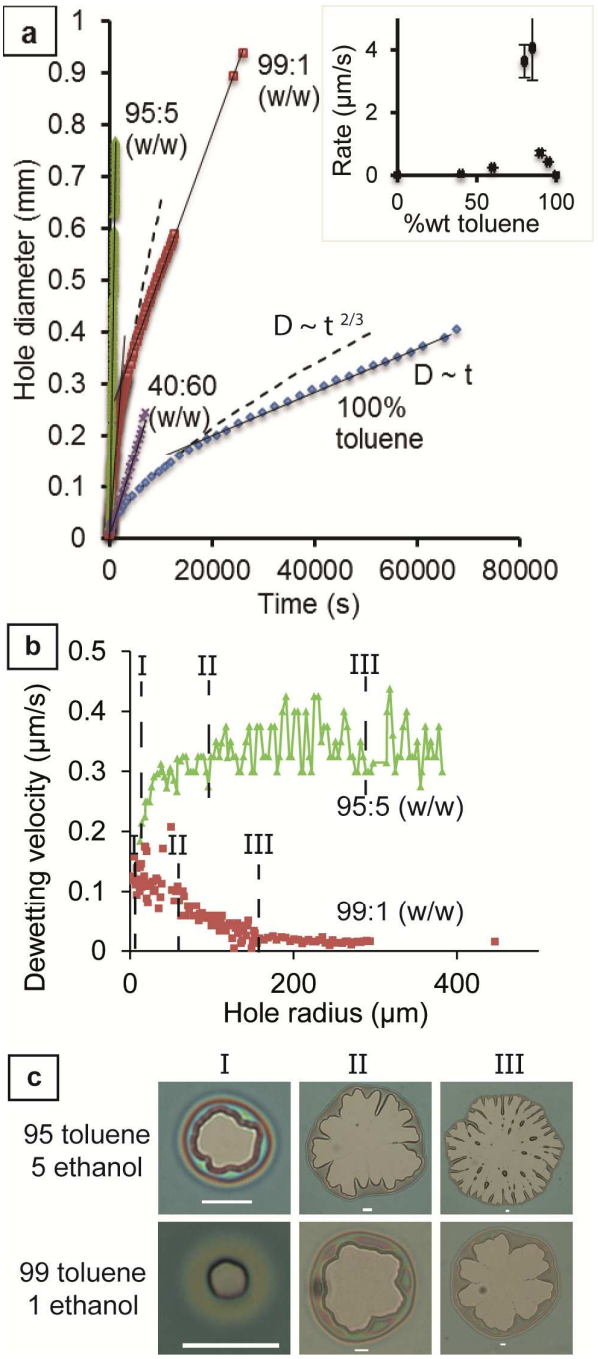


Figure 6: (a) Hole growth rate during dewetting of a 74.2 ± 0.8 nm thick PS96k film on a silicon substrate. The data is fitted by a power law $D \propto t^{2/3}$ at short times, and then as $D \propto t$ at later times. Inset: dewetting rate as a function of toluene content in the annealing solvent mixture. (b) Evolution of the dewetting velocity of the PS film when annealed in 99:1 (w/w) toluene/ethanol (red squares) and 95:5 (w/w) toluene/ethanol vapor (green triangles). (c) Optical micrographs of dewetted holes at three successive stages indicated in the text. Scale bars = 20 μm.

### *Dewetting thick polymer films*

To further demonstrate the strong drive for dewetting with toluene/ethanol mixtures, we annealed increasingly thicker films of a higher molecular weight polymer, PS192k, in the vapor mixture of 85:15 wt. toluene/ethanol. Strikingly, films of thickness from 100 nm to over 500 nm, very thick compared to expected range of action of interfacial forces ( < 100 nm), could be easily dewetted this way. Similar fingering behavior was observed as with thinner films (Figure 7a - d). As expected, droplet diameter increased with increasing film thickness, and droplets as large as 250 μm were produced (Figure 7e), with the density distribution of droplets decreasing accordingly. Dewetting rate decreased with increasing film thickness (Figure 7f), as expected, but still maintaining high values compared to the negligible dewetting that would occur in pure toluene.

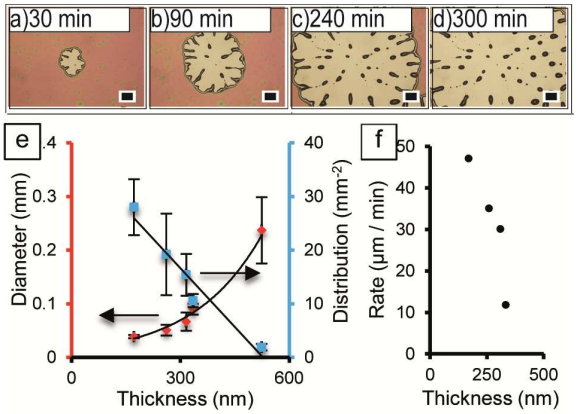


Figure 7: (a) – (d) Optical micrographs illustrating the dewetting of thick PS192k films (335 nm thick) in a mixture of 85:15 (w/w) toluene/ethanol, at room temperature (23 ± 1 °C), for the indicated times. Scale bars = 200 μm. (e) Average PS192k droplet diameter (red diamonds) and droplet distribution (blue squares) as a function of film thickness (lines are to guide the eye); (f) hole growth rate as a function of film thickness. Rate data was not collected for the 520 nm thick films as dewetting proceeded over a period of five days.

### *Reducing residual stress*

Thermally annealing polymer films for extended periods of time at temperatures below $T_g$ is known to reduce the elastic stress within the film, and lead to a decrease in hole nucleation density.[28, 33] Here, a PS96k film (75 nm thick) was thermally pre-annealed at 105 °C for 72 h (just above the bulk $T_g$ of PS) prior to annealing in a saturated environment of 80:20 wt. toluene/ethanol mixture (Figures 8a-c). The dewetting morphology and rate were compared with the dewetting of an untreated

film of the same thickness and molecular weight (Figures 8d-f). The holes in the thermally pre-treated film grew with a constant velocity that was approximately two orders of magnitude lower than that for untreated films (Figures 8g-h). These findings confirm earlier results that residual elastic stresses stored in the films provide an additional driving force for dewetting, and that when films are pre-equilibrated above $T_g$, these stresses may relax and the hole growth slows down. In these pre-equilibrated films the dewetting rates are still much larger than in pure toluene, so we can conclude that the additional elastic stress specifically due to the exposure to a good/non-solvent mixture contributes substantially to the dewetting forces.

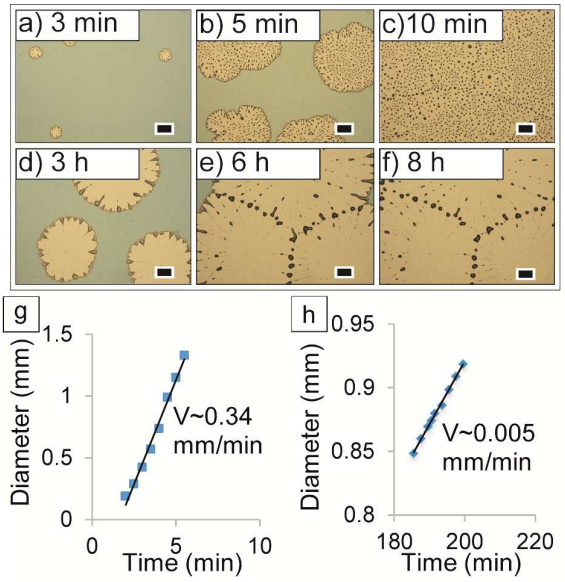


Figure 8: Thin PS96k film (76 ± 2 nm thick) annealed in the saturated vapor of 80:20 (w/w) toluene – ethanol mixture. (a-c) Film was solvent annealed as cast. (d-f) Film was thermally aged at 105°C for 72 h to reduce internal stress prior to annealing. Scale bars = 200 µm. Hole diameter as a function of annealing time of the (g) as cast, and (h) thermally pre-annealed films.

## Discussion

By collating all of the presented results, we can rationalize the effect of adding a small amount of ethanol to a toluene annealing environment for PS films. The investigated PS films did not dewet when annealed thermally and dewetted very slowly when exposed to pure toluene, but dewetted readily when even a small amount (2%) of ethanol was added. Our main conclusion is that annealing polystyrene films in good/non-solvent mixtures led to much stronger elastic recoiling forces than those usually observed when thermally annealing spin-cast films. This conclusion is substantiated in a few points below.

**Rim morphology and dewetted droplet shape –** The low contact angle of dewetted droplets and the shallow and wide rims obtained in pure toluene (Figure 4a) are a consequence of the conformation of the PS chains, which take on a loose, open coil confirmation, retained and locked-in even after the toluene vapor evaporates. The higher contact angle and the narrower and taller rims obtained when a small quantity of ethanol (1%) was added to the system are a consequence of the PS chains retracting into a compact globule conformation, as a result of the preferential adsorption of toluene in the vapor mixture. This peculiar situation could be thought of as an 'onion-like' structure: a core in which toluene molecules swell the PS chains, bridging together different chain segments, surrounded by an outer shell of ethanol, which ultimately drives the chain compaction (Figure 9). Our macro- and microscale observations are a consequence of the change in conformation of the polymer chains in the different solvents. To our knowledge, this is the first time that the collapse of the chains due to preferential adsorption of a good solvent in solvent mixture, as predicted by simulations,[45, 57] has been observed in a thin polymer film.

**Effect of adding ethanol on dewetting rate** – Upon addition of up to 15% wt. ethanol to toluene, the steady-state dewetting rate increased by more than two orders of magnitude (Figure 6b) compared to the pure toluene case. The bell- shaped curve of the average dewetting rate versus solvent mixture composition, with a maximum rate at 15% wt. concentration of ethanol (inset of Figure 6a), can be explained with the competition between the effects of the two solvents. The solvation of PS in toluene is required for dewetting to occur, as it plasticizes the chains and allows PS to flow (no dewetting was observed in pure ethanol vapor). The addition of ethanol drove the dewetting faster in two ways: on the one hand, by establishing polar interactions with the hydroxide groups on the silicon oxide substrate, which favor the spreading of ethanol and reduce the spreading parameter of PS. On the other hand, by reducing the PS viscosity, as a consequence of the collapsed and less entangled conformation of the PS chains, as will be discussed later. Increasing the amount of ethanol vapor above 15% wt. reduced the average dewetting velocity, due to reduced mobility of the chains, due to lower toluene content when dewetting started. Indeed, the uptake of the toluene in PS films has been seen to be considerably slowed down in an under-saturated atmosphere.[58] X-ray reflectometry data reinforce this explanation,

as at 30:70 wt. toluene/ethanol the swelling of the PS film was only 60% of the value obtained when annealing in pure toluene (Figure 2).

**Molecular recoiling forces** - Thermally pre-annealing the films close to $T_g$, and then exposing them to a mixed toluene/ethanol atmosphere, reduced the dewetting rate significantly. Very thick PS films - as thick as 520 nm - could be dewetted by annealing in toluene/ethanol vapor mixtures. The latter two observations point to strong elastic forces driving dewetting, in addition to the polar interactions at the interface.

Annealing the PS films above $T_g$ drives the chains away from their out-of-equilibrium 'frozen' conformation obtained through casting, towards more energetically favored quasi-equilibrium conformations.[27] This elastic rearrangement has been described in the past, particularly in ultra-thin films where elastic forces due to extreme confinement are strong.[59] Since the films prepared here had a thickness between $4R_g$ and $60R_g$, confinement effects were not very strong here, and it was instead the addition of the non-solvent ethanol that drove dewetting dramatically. Our observations are closely related to previous work by the Reiter and other groups on dewetting driven by relaxation of residual elastic stresses within the film.[28, 29, 33, 34, 42, 60, 61] However, in our study by introducing ethanol in the annealing environment, we substantially increased the recoiling forces in the rim region, and made the phenomenon more obvious.

**Transition from slip to no-slip regimes –** In all the vapor annealing situations investigated the hole growth followed the typical behavior expected for thin PS films dewetting upon thermal annealing (power law $D \sim t^{2/3}$ for slip dominated behavior, followed by a constant dewetting rate $D \sim t$ for a viscous dominated behavior).[16] However, when more than 1% wt. ethanol was added to the environment, the transition between the two regimes occurred at earlier times (Figure 6b).

According to accepted models,[16] in the initial dewetting period when the rim width is still growing, the dewetting velocity is dominated by interfacial slip, and is described by the power law $D \propto t^{2/3}$. In this regime the velocity is determined by:[17]

$$V_{slip} = \frac{1}{6}\frac{\gamma}{\eta}\theta^2\frac{b}{w}, \quad (3)$$

with $\gamma$ and $\eta$ the surface tension and viscosity of the liquid respectively, $\theta$ the contact angle of the liquid on the substrate, $b$ the slip length (the distance at which the velocity of the liquid extrapolates to zero) and $w$ the width of the rim. It is

straightforward to see from Equation (3) that as the rim width $w$ grows, there is a proportional reduction in dewetting velocity, and this regime is clearly visible for the 99:1 mixture (Figure 6b). Figure S3a shows clearly that $V_{slip}$ decreases with increasing rim width during toluene vapor annealing. Adding only 1 %wt. ethanol to the vapor environment results in the initial $V_{slip}$ decreasing not as strongly with increasing rim width (Figure S3b). Further addition of ethanol to the vapor mixture, results in $V_{slip}$ becoming independent of the rim width, suggesting possibly a change both in the interfacial properties of the substrate and the molecular properties of the polystyrene.

When $w = bL/\theta$, where $L$ is a constant of order 10,[62] the dynamics become viscosity-dominated, and slip is no longer the main dissipation mechanism. We were able to estimate slip length values from the value of rim width at which this transition from $R \propto t^{2/3}$ (slip) to $R \propto t$ (no-slip) occurs for the cases of annealing in pure toluene and in 95:5 (w/w) toluene/ethanol (in these two cases the viscosity could be approximated to be unchanged). The results are shown in Table 2. The value of slip length, $b$ = 700 nm, obtained for the 95:5 wt. toluene/ethanol case, is close to that obtained for PS dewetting on hydrophobised silicon OTS monolayers.[63] The increase in slip length on addition of ethanol is corroborated by the observation that the dewetted patterns in this case developed extensive fingering and droplet shedding, which is a signature of slip-dominated regimes.[21] Finally, it is expected that slip should become more dominant in situations, such as the mixed toluene/ethanol atmosphere, where the liquid wets the substrate less, and where the polymer coils are more compact and solid-like.[64, 65] By adding ethanol to the annealing mixture, we have effectively given a boost to the interfacial slip mechanism in the early stage of dewetting, in a manner that is more immediate and tunable than the modification of surface energy via self-assembled monolayers.[66, 67]

Table 2: Slip length and characteristic transition time from elastic to viscous dewetting regimes for PS96k films (75 nm thick) annealed in toluene and toluene/ethanol vapors. The derivation of the slip length is explained in the text, and that of transition times is explained in Figures S4 -S6 in SI.

| Annealing environment | Slip length, *b* (nm) | Characteristic time (s) |
|---|---|---|
| Pure toluene | 350 | 20 000 |
| 99:1 (w/w) toluene - ethanol | - | 3000 |
| 95:5 (w/w) toluene - ethanol | 700 | 270 |
| 60:40 (w/w) toluene - ethanol | - | 1000 |
| 40:60 (w/w) toluene – ethanol | - | 2000 |

**Film viscosity** – From our experiments a reptation time could be extracted (the time required for the polymer chain to completely emerge from its 'tube'[41, 42]), which is proportional to the viscosity of the polymer solution and its concentration. The time at which the hole growth rate in a dewetting film transitions from the slip-dominated to the viscous-dominated regime is proportional to the reptation time of the chains within the melt.[29] Table 2 shows the characteristic times at which this transition occurred for our films annealed in the different solvent mixtures (the selection of the transition rim width and time is described in detail in Figures S4-S6). For relatively constant toluene content, (100 % toluene, 99:1 wt. toluene/ethanol and 95:5 wt. toluene/ethanol) there is a two orders of magnitude decrease in characteristic transition time upon addition of ethanol. It is reasonable to consider that these transition times are proportional to the reptation time of the PS chains in the films, which can be attributed to two concurrent effects: an increase in interfacial slip due to adsorption of ethanol molecules to the substrate, and a reduction of polymer viscosity due to the collapse of the polymer chains and subsequent decrease in entanglement. It is not possible to distinguish and isolate these two effects, but it is likely they both play a role. The collapse of the polystyrene chain due to the preferential adsorption of toluene in the mixed vapor environment, was simulated by Magda in infinitely dilute solutions,[45] and is nicely replicated here, and partially explains the increased dewetting rate upon addition of ethanol. Figure 9 is a schematic summary of our observations, whereby the presence of ethanol in the solvent mixture results in dramatically increased dewetting rates and extensive fingering in the dewetted holes, due to the 'onion-like' structure of the toluene preferentially adsorbed to the PS chains within an ethanol shell.

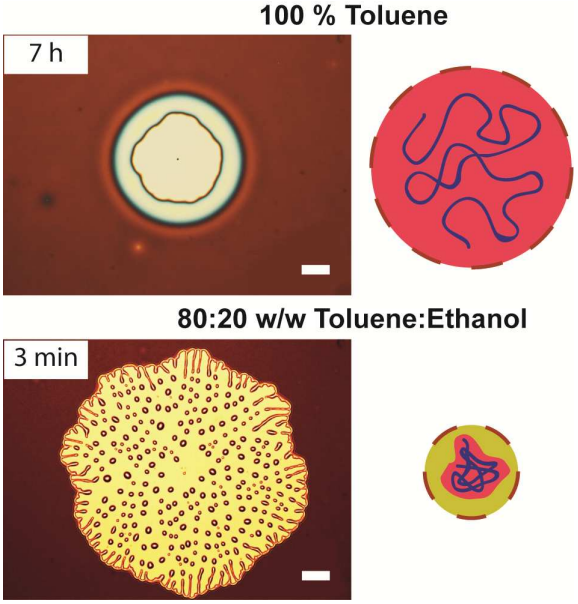


**Figure 9:** Schematic summary of these experiments: optical micrographs of a hole formed in a PS96k film (75 nm) dewetting in toluene vapor (above) after the indicated time of annealing, and in toluene/ethanol vapor mixture (below), scale bars = 200 μm; on the right corresponding chain conformations: swollen PS chain in toluene (red color), and collapsed chain in the solvent mixture (toluene red, ethanol yellow outside).

## Conclusions

In this paper we demonstrate that addition of ethanol vapor to a toluene vapor atmosphere affects drastically and on many levels the dewetting process of PS films. The consequences of adding up to 15% wt. ethanol to the toluene vapor atmosphere are: a reduced spreading parameter of the PS on the silicon oxide substrate, a reduced viscosity of the PS, an increased dewetting rate, a slip-dominated hole growth with extensive fingering, and the ability to dewet films as thick as 520 nm. The observed phenomena are attributed to the transition of the polymer chains to a globular conformation in a toluene/ethanol mixture, due to the strong preferential adsorption of the toluene. This behavior, predicted by Shultz and Flory,[44] and explored by numerical simulations by Magda *et al.*[45] for infinitely dilute polymer solutions, is much more pronounced in polymer melts. The addition of ethanol drives the dewetting faster, not only because the spreading parameter becomes more negative, but because the strong elastic recoiling forces on the chains drive hole growth and interfacial slip is increased. From an application point of view, annealing metastable films in mixed solvent vapors is a convenient and tunable way to produce very large

dewetted droplets, and to tune the dewetting dynamics more strongly towards a slip regime, without the need for surface modification.

## Acknowledgements

C.N. acknowledges the Australian Research Council for funding, and the Bragg Institute (ANSTO) for beam time.

**Supporting Information**

Hansen solubility parameters for toluene and ethanol with respect to PS, optical micrograph of a metastable PS film thermally annealed, molar composition of the toluene/ethanol vapor mixtures, growth of rim width versus time, identification of the characteristic transition times. This material is available free of charge via the Internet at http://pubs.acs.org.

## References

1. de Gennes, P. G., *Rev. Mod. Phys.* **1985,** 57, 827-863.
2. Srolovitz, D. J.; Safran, S. A., *J. Appl. Phys.* **1986,** 60, 255-260.
3. Reiter, G., *Phys. Rev. Lett.* **1992,** 68, (1), 75-78.
4. Xie, R.; Karim, A.; Douglas, J. F.; Han, C. C.; Weiss, R. A., *Phys. Rev. Lett.* **1998,** 81, (6), 1251-1254.
5. Saulnier, F.; Raphaël, E.; de Gennes, P.-G., *Phys. Rev. E* **2002,** 66, (6), 061607.
6. Seemann, R.; Herminghaus, S.; Neto, C.; Schlagowski, S.; Podzimek, D.; Konrad, R.; Mantz, H.; Jacobs, K., *J. Phys.: Condens. Matter* **2005,** 17, (9), S267.
7. Bäumchen, O.; Jacobs, K., *J. Phys.: Condens. Matter* **2010,** 22, (3), 033102.
8. Gentili, D.; Foschi, G.; Valle, F.; Cavallini, M.; Biscarini, F., *Chem. Soc. Rev.* **2012,** 41, (12), 4430-4443.
9. Xue, L.; Han, Y., *Prog. Polym. Sci.* **2011,** 36, (2), 269-293.
10. Thickett, S. C.; Moses, J.; Gamble, J. R.; Neto, C., *Soft Matter* **2012,** 8, (39), 9996-10007.
11. Telford, A.; Meagher, L.; Glattauer, V.; Gengenbach, T.; Easton, C.; Neto, C., *Biomacromolecules* **2012,** 13, (9), 2989-2996.
12. Ghezzi, M.; Wang, P.-Y.; Kingshott, P.; Neto, C., *Adv. Mater. Interfaces* **2015,** 2, (11).
13. Thickett, S. C.; Neto, C.; Harris, A. T., *Adv. Mater.* **2011,** 23, (32), 3718-3722.
14. Seemann, R.; Herminghaus, S.; Jacobs, K., *Phys. Rev. Lett.* **2001,** 86, (24), 5534-5537.
15. Brochard-Wyart, F.; Redon, C., *Langmuir* **1992,** 8, (9), 2324-2329.
16. Brochard-Wyart, F.; de Gennes, P.-G.; Hervert, H.; Redon, C., *Langmuir* **1994,** 10, (5), 1566-1572.
17. Reiter, G.; Sharma, A., *Phys. Rev. Lett.* **2001,** 87, (16), 166103.

18. Münch, A.; Wagner, B., *J. Phys.: Condens. Matter* **2011,** 23, (18), 184101.
19. Münch, A.; Wagner, B., *Physica D* **2005,** 209, 178-190.
20. Reiter, G., *J. Adhesion* **2005,** 81, (3-4), 381-395.
21. Bäumchen, O.; Marquant, L.; Blossey, R.; Münch, A.; Wagner, B.; Jacobs, K., *Phys. Rev. Lett.* **2014,** 113, (1), 014501.
22. Sharma, A., *Langmuir* **1993,** 9, (3), 861-869.
23. Sharma, A.; Khanna, R., *Phys. Rev. Lett.* **1998,** 81, (16), 3463-3466.
24. Reiter, G., *Phys. Rev. Lett.* **2001,** 87, (18), 186101.
25. Reiter, G.; de Gennes, P. G., *Eur. Phys. J. E* **2001,** 6, (1), 25-28.
26. Bollinne, C.; Cuenot, S.; Nysten, B.; Jonas, A. M., *Eur. Phys. J. E* **2003,** 12, (3), 389-396.
27. Yang, M.; Hou, S.; Chang, Y.; Yang, A.-M., *Phys. Rev. Lett.* **2006,** 96, (6), 066105.
28. Reiter, G.; Hamieh, M.; Damman, P.; Sclavons, S.; Gabriele, S.; Vilmin, T.; Raphaël, E., *Nat. Mater.* **2005,** 4, (10), 754-758.
29. Damman, P.; Gabriele, S.; Coppée, S.; Desprez, S.; Villers, D.; Vilmin, T.; Raphaël, E.; Hamieh, M.; Al Akhrass, S.; Reiter, G., *Phys. Rev. Lett.* **2007,** 99, (3), 036101.
30. Thomas, K. R.; Steiner, U., *Soft Matter* **2011,** 7, 7839.
31. Ediger, M. D.; Forrest, J. A., *Macromolecules* **2014,** 47, (2), 471-478.
32. Barbero, D. R.; Steiner, U., *Phys. Rev. Lett.* **2009,** 102, (24), 248303.
33. Thomas, K. R.; Chenneviere, A.; Reiter, G.; Steiner, U., *Phys. Rev. E* **2011,** 83, (2), 021804.
34. Clough, A.; Chowdhury, M.; Jahanshahi, K.; Reiter, G.; Tsui, O. K. C., *Macromolecules* **2012,** 45, (15), 6196-6200.
35. Raegen, A.; Chowdhury, M.; Calers, C.; Schmatulla, A.; Steiner, U.; Reiter, G., *Phys. Rev. Lett.* **2010,** 105, (22), 227801.
36. Lee, S. H.; Yoo, P. J.; Kwon, S. J.; Lee, H. H., *J. Chem. Phys.* **2004,** 121, (9), 4346-4351.
37. Xu, L.; Shi, T.; An, L., *Langmuir* **2007,** 23, (18), 9282-9286.
38. Xu, L.; Shi, T.; An, L., *J. Chem. Phys.* **2008,** 129, (4), 044904.
39. Burtovyy, R.; Luzinov, I., *Langmuir* **2008,** 24, (11), 5903-5910.
40. Xu, L.; Sharma, A.; Joo, S. W., *Macromolecules* **2012,** 45, (16), 6628-6633.
41. de Gennes, P.-G., *Scaling Concepts in Polymer Physics*. Cornell University Press: 1979.
42. Grosberg, A. Y.; Khokhlov, A., *Statistical Physics of Macromolecules*. American Institute of Physics: New York, 1994; p 1-144.
43. Baysal, B. M.; Karasz, F. E., *Macromol. Theory Simul.* **2003,** 12, (9), 627-646.
44. Shultz, A.; Flory, P., *J. Polym. Sci.* **1955,** 15, (79), 231-242.
45. Magda, J.; Fredrickson, G.; Larson, R.; Helfand, E., *Macromolecules* **1988,** 21, (3), 726-732.
46. Nakata, M., *Phys. Rev. E* **1995,** 51, (6), 5770.
47. Auroy, P.; Auvray, L., *Macromolecules* **1992,** 25, (16), 4134-4141.
48. Hansen, C. M., *Hansen Solubility Parameters: a User's Handbook*. CRC press: 2007.
49. Kretschmer, C. B.; Wiebe, R., *J. Am. Chem. Soc.* **1949,** 71, (5), 1793-1797.
50. Brandrup, J.; Immergut, E., *Polymer Handbook*. John Wiley & Sons, New York, NY: 1975.
51. O'Driscoll, S.; Demirel, G.; Farrell, R. A.; Fitzgerald, T. G.; O'Mahony, C.; Holmes, J. D.; Morris, M. A., *Polym. Adv. Technol.* **2011,** 22, (6), 915-923.

52. *Solid surface energy data for common polymers*; DataPhysics Instruments: 2006.
53. Seemann, R.; Herminghaus, S.; Jacobs, K., *J. Phys.: Condens. Matter* **2001,** 13, (21), 4925.
54. The dewetting velocity is taken to be the steady state value reached when fingering and droplet shedding was well-established. The details of instantaneous rate change for all mixtures can be appreciated in Figure S2.
55. Jacobs, K.; Seemann, R.; Schatz, G.; Herminghaus, S., *Langmuir* **1998,** 14, 4961-4963.
56. For the dewetting rate on irregularly shaped holes, the following procedure was followed: the area inside the hole was obtained by the software based on grey scale contrast, the equivalent radius of a circular area derived, and the instantaneous velocity was obtained by the change in radius over two adjacent images, typically 10 seconds apart.
57. Termonia, Y., *J. Polym. Sci., Part B: Polym. Phys.* **1999,** 37, (19), 2782-2787.
58. Mueller-Buschbaum, P.; Bauer, E.; Maurer, E.; Nelson, A.; Cubitt, R., *Phys. Status Solidi* **2007,** 1, (2), 68-70.
59. Zhao, W.; Rafailovich, M.; Sokolov, J.; Fetters, L.; Plano, R.; Sanyal, M.; Sinha, S.; Sauer, B., *Phys. Rev. Lett.* **1993,** 70, (10), 1453.
60. Gabriele, S.; Sclavons, S.; Reiter, G.; Damman, P., *Phys. Rev. Lett.* **2006,** 96, (15), 156105.
61. Vilmin, T.; Raphael, E., *Eur. Phys. J. E* **2006,** 21, 161-174.
62. Redon, C.; Brochard-Wyart, F.; Rondelez, F., *Phys. Rev. Lett.* **1991,** 66, (6), 715.
63. Fetzer, R.; Jacobs, K., *Langmuir* **2007,** 23, (23), 11617-11622.
64. Neto, C.; Evans, D. R.; Bonaccurso, E.; Butt, H.-J.; Craig, V. S. J., *Rep. Prog. Phys.* **2005,** 68, 2859-2897.
65. Lee, T.; Charrault, E.; Neto, C., *Adv. Colloid Interface Sci.* **2014,** 210, (0), 21-38.
66. Haefner, S.; Benzaquen, M.; Bäumchen, O.; Salez, T.; Peters, R.; McGraw, J. D.; Jacobs, K.; Raphael, E.; Dalnoki-Veress, K., *Nat Commun* **2015,** 6, 7409.
67. Choi, S.-H.; Zhang Newby, B., *J. Chem. Phys.* **2006,** 124, 54702.